



# Modeling and simulation of an isolated mini-grid including battery operation strategies under uncertainty using chance constraints

Nina Kliche<sup>1</sup> · René Henrion<sup>1</sup> · Dietmar Hömberg<sup>1,2,3</sup>

Received: 2 September 2024 / Accepted: 12 August 2025

© The Author(s), under exclusive licence to Springer-Verlag GmbH Germany, part of Springer Nature 2025

## Abstract

This paper addresses the challenge of handling uncertainties in mini-grid operation, crucial for achieving universal access to reliable and sustainable energy, especially in regions lacking access to a national grid. Mini-grids, consisting of small-scale power generation systems and distribution infrastructure, offer a cost-effective solution. However, the intermittency and uncertainty of renewable energy sources poses challenges, mitigated by employing batteries for energy storage. Optimizing the lifespan of the battery energy storage system is critical, requiring a balance between degradation and operational expenses, with battery operation strategies playing a key role in achieving this balance. Accounting for uncertainties in renewable energy sources, demand, and ambient temperature is essential for reliable energy management strategies. By formulating a probabilistic optimal control problem for minimizing the daily operational costs of stand-alone mini-grids under uncertainty, and exploiting the concept of joint chance constraints, we address the uncertainties inherent in battery dynamics and the associated operational constraints.

**Keywords** Mini-grid operation · Uncertainty management · Risk management · Probabilistic optimal control

## Abbreviations

BESS	Battery energy storage system
BTMS	Battery thermal management system
CCC	Cycling chance constraint
DG	Diesel generator
DOD	Depth-of-discharge
ECM	Equivalent circuit model

---

R. Henrion and D. Hömberg contributed equally to this work.

---

Extended author information available on the last page of the article

JCC	Joint chance constraint
LIB	Lithium-ion battery
OCp	Optimal control problem
ODE	Ordinary differential equation
PL	Probability level
PV	Photovoltaic
RES	Renewable energy source
SOC	State-of-charge
SOH	State-of-health

## 1 Introduction

As outlined by the United Nations, 675 million people still lack access to electricity with four out of five residing in sub-Saharan Africa. As an immediate consequence, one sustainable development goal aims at ensuring universal access to affordable, reliable, sustainable and modern energy. This goal encapsulates two primary tasks. The first task is to prioritize universal access to electricity, ensuring that every individual has the fundamental right to reliable power. The secondary task entails decarbonizing the energy sector, transitioning towards cleaner and more sustainable sources of power. A concrete example is rural Ethiopia, where 70 % of the population lacks reliable access to electricity. Extending the main grid is prohibitively expensive such that mini-grids – localized energy networks – emerge as a cost-effective and dependable solution. They typically consist of small-scale power generation systems and distribution infrastructure which potentially has connection to the main grid. The typical installation includes a back-up diesel generator and utilizes some renewable energy source (RES), for instance photovoltaic (PV) or wind, aligning with the goal of decarbonizing electricity. However, the intermittency and uncertainty of RES poses challenges. To mitigate this, batteries are employed. They serve to store excess power when available and provide it during periods of insufficient output from RES [1] as well as to stabilize the mini-grid as they can buffer uncertainties in both generation and consumption.

The integration of a battery energy storage system (BESS) is crucial to address as we navigate towards a sustainable and reliable energy future [2] and investment and replacement costs are of critical concern as we aim at striking a balance between affordability and quality. The concept of second-life lithium-ion batteries (LIBs) emerges as a promising solution: by re-purposing LIBs, we can significantly decrease investment costs while simultaneously strengthening sustainability efforts. In this regard, the lifespan of a BESS holds considerable significance. Understanding and optimizing longevity ensures that investments yield lasting benefits, aligning with our sustainability goals. On that account, we aim at operating the BESS in a manner that strikes balance between minimizing degradation alongside operational expenses. Degradation is closely related to the state-of-health (SOH) of a battery. Although there is no uniform definition for the SOH of a battery it still can be quantified in terms of resistance increase and capacity decrease. There are two main aging mechanisms, namely calendar and cycle aging. Calendar aging is the aging mechanism hap-

pening when at rest while cycle aging is the aging mechanism happening when in use. During cycle aging, calendar aging still occurs. It is observed that depth-of-discharge (DOD) and temperature both exhibit a significant influence on battery degradation. Higher DODs and higher temperatures lead to faster degradation over time in both capacity and resistance resulting in both capacity and power loss, respectively [3, 4]. Oversizing of a BESS is a viable but very costly solution to prevent high DODs and high temperatures. For this very reason, a battery operation strategy can become key in achieving an optimal trade-off between minimal degradation and optimal operational costs [5]. Thus, tailoring battery operation strategies to the specific demands of the application ensures that LIBs operate optimally and have an extended lifespan.

Another important characteristic of mini-grid management is the presence of uncertainty as naturally introduced by RES, demand and ambient temperature. While these elements can be predicted to some extent, accounting for forecast errors is crucial for a reliable and resilient energy management strategy.

This paper tackles a key challenge in mini-grid operation: handling uncertainties. An energy management strategy for minimizing the daily operational costs of a stand-alone mini-grid under uncertainty is presented. The proposed energy management considers a predefined mini-grid layout and takes into account a prescribed battery (thermal) operation strategy. Building upon this design, a probabilistic optimal control problem (OCP) is set up and solved numerically. The OCP includes state equations describing battery dynamics in form of a coupled ordinary differential equation and state constraints, i.e. ranges for battery temperature and state-of-charge (SOC), corresponding to the battery (thermal) operation strategy. Due to the presence of uncertainty such as solar energy, energy demand and ambient temperature, the state constraints become uncertain. As our decisions on optimal dispatch of the mini-grid have to be optimized and applied prior to the realization of uncertainty, it is reasonable to formulate probabilistic state constraints in which a decision is declared to be feasible whenever the random state constraints are satisfied with at least some given probability.

A good overview of battery models on various scales can be found in the recent monograph [6], while [7] surveys battery energy storage models and control strategies for the optimal operation of a BESS. Further approaches for optimal BESS operation based on time-discrete state equations can be found, e.g., in [8–11]. Probabilistic or chance constraints have been introduced in [12] (see also the fundamental monograph [13]). Substantial progress in the development of numerical approaches for dealing with chance constraints has been made in the last twenty years. We mention here the methods of *scenario approximation* [14], *sample average approximation* [15], *convex approximation* [16], *difference-of-convex-functions (DC) approximation* [17], *smooth approximation* [18, 19], *kernel density estimators* [20, 21], *spherical-radial decomposition* [22], *importance sampling* [23], or *bilevel optimization* [24].

In the context of mini-grids, chance constraints have been considered, for instance, in [25, 26], who investigated the so-called *probability of successful islanding* when, due to a possible outage of the main grid, a mini-grid has to survive in isolated mode for a certain period of time with a given probability. In those papers, the chance constraints were formulated point-wise in time. Though point-wise (or: individual) constraints are easy to deal with at least in the models of these papers, one has to be

aware of that pointwise high probability may potentially result in a low probability of satisfying the corresponding constraints over the whole time horizon. Therefore, so-called *joint chance constraints* are preferred in general, but coming at the price of more sophisticated analysis and numerics because of dealing with multivariate distributions. Here, the probability of satisfying constraints simultaneously over the whole time horizon is controlled.

In a recent paper [27], joint chance constraints were considered in the context of probability of successful islanding of weakly connected mini-grids and the advantages over point-wise constraints became clearly visible. At the same time, in this and many related papers dealing with chance constraints, the battery operation was modeled in quite an elementary manner. In the simplest case, degradation costs are just measured proportionally to charge and discharge. The main novelty of the present paper consists in combining joint chance constraints with a more realistic model of battery operation based on a coupled system of ODEs as mentioned above. The resulting physical states (state of charge and temperature) are supposed to stay within given limits at high probability (with respect to the present uncertainties) throughout the considered time horizon (joint chance constraint). Mathematically, this leads to the challenge of treating chance constraints in the framework of differential equations. Our working horse in this respect is the *spherical-radial decomposition* of Gaussian random vectors which has been well analyzed theoretically and successfully applied in the past to numerous problems of operations research (see [22, 27–30]). Its main advantage is the precision in probability estimation and the characterization of the theoretical and estimated (sub-)gradient of the underlying probability function. Both is possible thanks to exploiting structural information about elliptical, in particular Gaussian distributions. This appealing aspect, however, comes with an increased complexity of estimating the so-called radial probability, in particular when passing from simple explicit inequality constraints (as in operations research) to random state constraints in differential equations.

The paper is organized as follows. Section 2 is dedicated to modeling the power balance, the BESS and the uncertainties. In Section 3 the desired probabilistic OCP will be derived. Section 4 gives details on how to compute probabilities and their derivatives by means of the spherical-radial decomposition. In Section 5 the proposed OCP is solved numerically. Results are given followed by a critical discussion and an outlook.

## 2 Modeling

### 2.1 Power balance

The power balance states that power supply and consumption must always be in equilibrium at any time  $t$  with power measured in watts (W). It is given in the form of the algebraic equation  $P_{in} = P_{out}$ . For a stand-alone mini-grid it reads according to Figure 1,

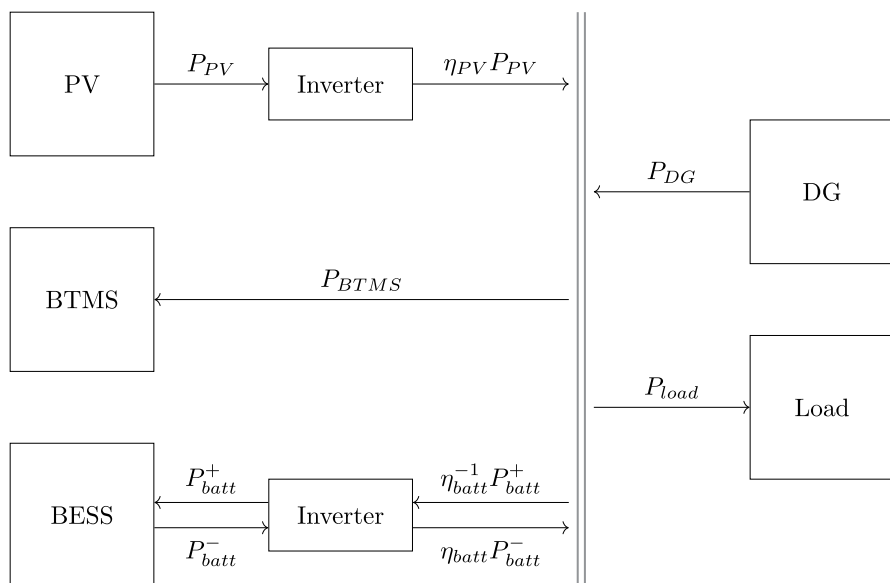


**Fig. 1** A simplified depiction of the installation of a mini-grid and its corresponding power flow. On the left hand-side, the direct current sources and sinks are depicted. On the right hand-side, the alternate current sources and sinks are illustrated. The double-dash line represents the distribution infrastructure where the power balance must hold at any time. The excess power  $P_{dump}$  is not part of this illustration but must not be neglected in the power balance.

$$\eta_{PV} P_{PV} + \eta_{batt} P_{batt}^- + P_{DG} = P_{load} + \frac{1}{\eta_{batt}} P_{batt}^+ + P_{BTMS} + P_{dump} \quad (1)$$

with  $P_{PV}$  the PV power,  $P_{DG}$  the power provided by the back-up Diesel generator (DG) and  $P_{load}$  the demand.  $P_{batt} = P_{batt}^+ - P_{batt}^-$  corresponds to battery power with  $P_{batt}^+$  the charging and  $P_{batt}^-$  the discharging power. The  $P_{BTMS}$  represents the power needed by the battery thermal management system for cooling or heating. The model also accounts for excess power  $P_{dump}$ , which may occur when there is a power surplus and the BESS is fully charged. In this planning context,  $P_{dump}$  acts as a modeling abstraction to capture scenarios of renewable energy surplus. While this abstraction simplifies planning, it represents potential curtailment or safeguards that would be implemented in a real-world system to ensure grid stability. The inverter efficiencies  $\eta_{batt}$ ,  $\eta_{PV} < 1$  are assumed to be constant in this work.

## 2.2 Modeling of the battery energy storage system

In the following section, we introduce a model that combines a battery model with a temperature model for a BESS. A BESS consists of several battery packs which, in turn, consist of several battery modules connected in series and parallel. Battery modules are made of battery cells also connected in series and parallel. The exact topology is usually determined by economic and safety considerations and shall not be discussed in this work. Instead, we consider a generic BESS consisting of  $N$  bat-

tery cells. Electric power is computed as the product of current and voltage, i.e. for a single cell  $P_{cell}(t) = V(t) \cdot I(t)$  and for a BESS consisting of  $N$  cells

$$P_{batt}(t) = N \cdot P_{cell}(t) = N \cdot V(t) \cdot I(t). \quad (2)$$

We now seek describing equations for the voltage and the current of a battery cell as well as equations describing the dynamics of such a cell.

Battery features as e.g. voltage responses, are often and usually approximated using equivalent circuits. An electric circuit serves as an analogue to predict battery's behavior [6]. More precisely, we use a charge reservoir model [6, 7] that defines capacity in units of ampere-hours (Ah). For a day-ahead optimization with a forecast horizon of one day and low time resolution, a  $0^{th}$  order equivalent circuit model (ECM), cf. Figure 2, is appropriate and sufficient [7]. By Kirchhoff's law, see for instance [31], the terminal voltage  $V$ , measured in volts (V), is given by

$$V(t) = V_{OC} + R_{\tau}I(t) \quad (3)$$

with  $V_{OC}$  the open circuit voltage (OCV),  $R_{\tau}$  the internal resistance measured in ohms ( $\Omega$ ) and  $I$  the current flowing through the battery measured in ampere (A). We write

$$I(t) = I^+(t) - I^-(t) = \begin{cases} > 0 & \text{for charging} \\ < 0 & \text{for discharging} \end{cases} \quad I^{\pm} \geq 0,$$

where we have agreed on the notation  $I^+ = \max\{0, I\}$  the positive part and  $I^- = \max\{0, -I\}$  the negative part. The OCV is the terminal voltage of the battery when measured at rest, i.e. when the current is zero. The OCV is a function of SOC, SOH and battery temperature. In the following, we will assume  $V_{OC} = V_{OC}(SOC)$  as we assume on the one hand the variations w.r.t. to SOH to be small and on the other

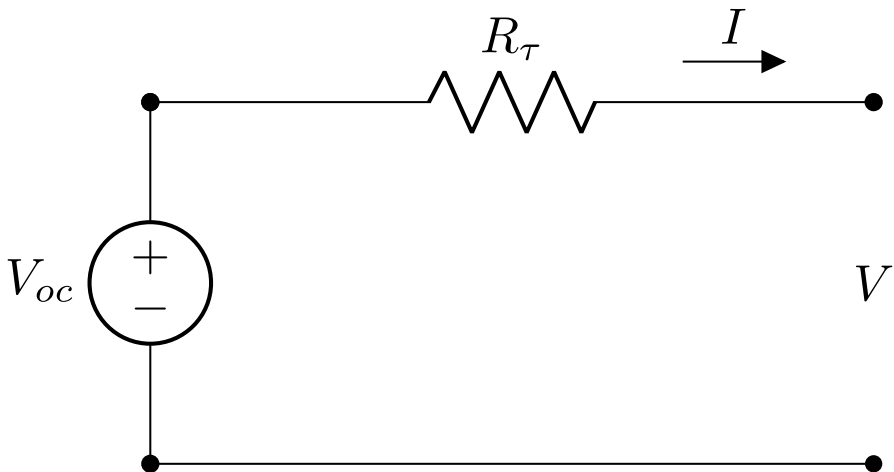


Fig. 2  $0^{th}$  order equivalent circuit model

hand, we operate in a temperature-controlled environment such that we may neglect temperature dependency. From [3], the OCV can be fitted to a function in  $SOC$ , cf. Figure 3. The nominal internal resistance  $R_0$  typically is part of the manufacturer's specifications. The progressive increase of resistance over time is one facet of battery degradation. The higher the internal resistance, the higher the voltage drop across the battery such that, eventually, increase in resistance due to degradation translates into power loss. The degraded resistance is denoted by  $R_\tau$ . The gradual loss of capacity over time is another facet of battery degradation. The capacity of a battery indicates the amount of electric charge that a battery can deliver or store according to the manufacturer's specifications. It is given as the nominal capacity  $Q_0$  measured in ampere-hours for a new battery. In the following, the degraded capacity of a second-life battery will be denoted by  $Q_\tau$ .

The SOC is quantified as the ratio of available capacity and degraded (total) capacity. The SOC of a  $0^{th}$  order ECM can be modeled by means of Coulomb counting, i.e. integrating the current over time.

$$SOC(t) = \frac{Q(t)}{Q_\tau} = SOC(t_0) + \int_{t_0}^t \frac{I(s)}{Q_\tau} ds.$$

This yields the dynamics for the SOC,

$$Q_\tau SOC'(t) = I(t) = \text{C-rate} \cdot \frac{Q_0}{1h}. \quad (4)$$

At this point, the C-rate has been introduced, too. The C-rate quantifies the rate at which a battery is charged or discharged in relation to its nominal capacity and is defined as the inverse of the time it takes, in hours (h), to fully discharge a battery.

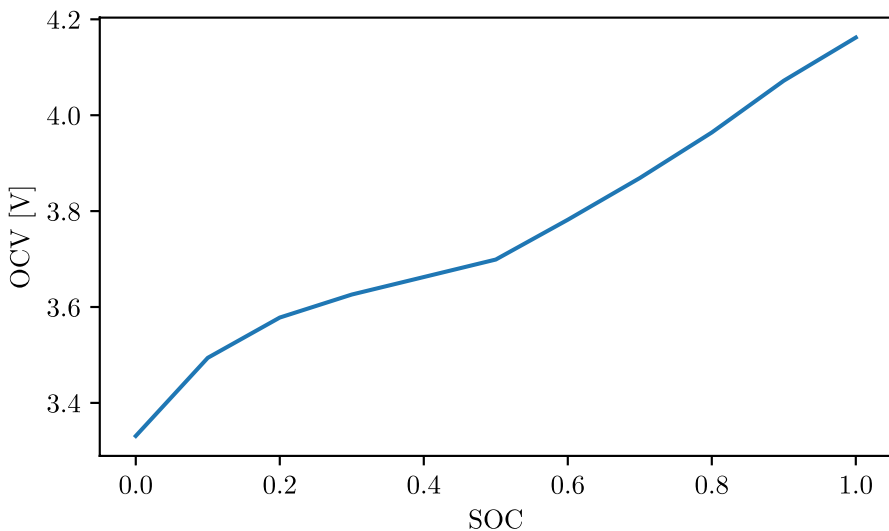


**Fig. 3** Open-circuit voltage as a function of state-of-charge

Given the  $0^{th}$  order ECM, equations for the battery temperature evolution can be set up by means of Newton's law of cooling yielding an ODE, see for instance [7]. The temperature of a battery is a function of heat generated by the battery through operation and the heat exchange between the battery and its environment and typically is given in units of Kelvin (K). For the considered  $0^{th}$  order ECM, the heat generated by the battery that is taken into account is the Joule heating. Heat is generated (or consumed) in further ways, which will be neglected in the following as they are comparably small [7]. The rate at which heat is transferred through a material is given by [31]

$$\frac{\lambda A}{l} \Delta T = U A \Delta T$$

with  $l$ , given in meters (m), representing material thickness,  $\lambda$  measured in  $W/m \cdot K$  the thermal conductivity and  $A$  the exposed material surface area (the "interface") given in units of  $m^2$ . Eventually, we call  $U$  the thermal transmittance which is given in units of  $W/m^2 \cdot K$ .

In a mini-grid application, several battery packs are stored in an enclosure. This means that there must be a separation of the weather-dependent environment and the actual environment the batteries are operating in. We thus seek a coupled ODE describing battery cell and battery enclosure temperature. To regulate the battery cell temperature, we introduce a BTMS. Denote  $T_{cell}$  the battery cell temperature,  $T_{en}$  the enclosure temperature and  $T_{amb}$  the ambient temperature. The battery temperature then evolves, by Newton's law of cooling, according to the following coupled ODE,

$$C_{cell} T'_{cell}(t) = R_{\tau} I^2 + U_{cell} (T_{en} - T_{cell}) \quad (5a)$$

$$C_{en} T'_{en}(t) = \eta_{BTMS} P_{BTMS} + N \cdot U_{cell} (T_{cell} - T_{en}) + U_{en} (T_{amb} - T_{en}) \quad (5b)$$

with  $Q_{BTMS} = \eta_{BTMS} P_{BTMS}$  the thermal power given as a fraction of the electric power  $P_{BTMS}$  needed for cooling. This approach assumes a constant air velocity and can be further developed by adding a fan and a heat exchanger.  $C_{cell}$ ,  $C_{en}$  are the battery and enclosure heat capacity, respectively, while  $U_{cell}$ ,  $U_{en}$  denote their battery and enclosure thermal conductances.  $N$  refers to the number of battery cells the BESS consists of.

In this work, a high energy 18650 lithium-ion cylindrical battery cell manufactured by Sanyo, labeled UR18650E has been considered. The cell specifications according to the data sheet as well as some thermodynamic properties are summarized in Table 1. Some thermodynamic parameters of the battery enclosure are listed in Table 2. Note that the thermodynamic parameters are not meant to represent a specific

**Table 1** Cell specification and thermodynamic properties

Description	Symbol	Value
Nominal capacity	$Q_0$	2.05 Ah
Battery specific heat capacity	$c_{cell}$	890 J/kg · K [32]
Battery thermal transmittance	$\lambda_{cell}$	0.2 W/m · K [33]



**Table 2** Thermodynamic properties of battery enclosure

Description	Symbol	Value
Enclosure heat capacity	$C_{en}$	63 kJ/W [7]
Enclosure thermal conductance	$U_{en}$	0.45 W/m <sup>2</sup> · K

enclosure topology. Instead, we assume that the BESS consists of well-insulating materials.

### 2.3 Modeling the uncertainties

For a day-ahead optimization, we consider uncertainties in the forecasts of PV power, demand and ambient temperature. Using historical data, future values can be forecasted coming at the price of prediction errors. We thus represent  $x_t = \hat{x}_t + \xi_t$ , where  $\hat{x}_t$  corresponds to the deterministic forecast and  $\xi_t$  to the uncertain prediction error.

Causal and invertible ARMA( $p, q$ ) processes can be forecasted up to some prediction error [34]. A time series  $\{x_t\}_t$  is called an ARMA( $p, q$ ) process if  $x_t + \sum_{j=1}^p \phi_j x_{t-j} = \omega_t + \sum_{j=1}^q \theta_j \omega_{t-j}$  where  $\omega_t \sim \text{iid } \mathcal{N}(0, \sigma_\omega^2)$ . An ARMA( $p, q$ ) model is said to be causal if  $x_t = \sum_{j=0}^{\infty} \psi_j \omega_{t-j}$ ,  $\psi_0 = 1$  with  $\sum_{j=0}^{\infty} |\psi_j| < \infty$ . The  $\psi$ -weights of a causal ARMA( $p, q$ ) process satisfy

$$\begin{cases} \psi_j + \sum_{k=1}^p \phi_k \psi_{j-k} = 0 & \text{if } j \geq \max(p, q+1) \\ \psi_j + \sum_{k=1}^p \phi_k \psi_{j-k} = \theta_j & \text{if } 0 \leq j \leq \max(p, q+1). \end{cases} \quad (6)$$

An ARMA( $p, q$ ) model is said to be invertible if  $\omega_t = \sum_{j=0}^{\infty} \pi_j x_{t-j}$ ,  $\pi_0 = 1$  with  $\sum_{j=0}^{\infty} |\pi_j| < \infty$  and the  $\pi$ -weights of an invertible ARMA( $p, q$ ) satisfy an analogue to Equation (6).

Let  $\{x_t\}_t$  be a causal and invertible ARMA( $p, q$ ) process. Assume there exists a complete history of measurements  $\{x_0, x_{-1}, x_{-2}, \dots\}$ . It holds  $x_t = \hat{x}_t + \xi_t$  with  $\hat{x}_t$  the prediction and  $\xi_t$  the prediction error. More precisely,

$$\begin{aligned} \hat{x}_t &= - \sum_{j=1}^{t-1} \pi_j \hat{x}_{t-j} - \sum_{j=t}^{\infty} \pi_j x_{t-j} \\ \xi_t &= \sum_{j=0}^{t-1} \psi_j \omega_{t-j} \end{aligned}$$

and the prediction errors are correlated with  $\text{cov}(\xi_t, \xi_{t+m}) = \mathbb{E}(\xi_t \xi_{t+m}) = \sigma_\omega^2 \sum_{j=0}^{m-1} \psi_j \psi_{j+m}$ .

While no specific historical dataset was used to derive the model representation, the ARMA( $p, q$ ) framework is well-suited for this application due to its ability to capture the stochastic nature of prediction errors. This choice emphasizes the general applicability of the approach rather than reliance on a particular dataset, providing a theoretical foundation for incorporating forecast uncertainty into the optimization process.

### 3 Optimal control formulation

Given a battery and a battery temperature model, a probabilistic OCP that aims at minimizing the daily operational costs subject to a battery (thermal) operation strategy will be proposed. The probabilistic OCP takes into account the uncertainties introduced by PV power, demand and ambient temperature, yielding a reliable energy management strategy. We proceed in the following manner. In a first step, a deterministic OCP for minimizing the daily operational costs of an isolated mini-grid will be introduced. In a second step, it will be discussed how one can deal with the uncertainties and the approach taken in this work will be described. In a last step, the discretized OCP considered in this work will be established.

The operational costs of a stand-alone mini-grid are determined by fuel consumption of the back-up DG, mitigating financial expenses as well as environmental impact. Without knowledge of the exact DG, we decide to minimize the total DG power. Motivated by the fact that excess power is undesirable as it can affect the stability of a mini-grid, cf. [35], one could also consider penalizing dumping excess power.

#### 3.1 Deterministic problem formulation

For a day-ahead optimization the goal is to find an optimal energy management strategy that minimizes the operational costs. In the off-grid case, this translates into minimizing diesel fuel consumption. The optimization is subject to the algebraic power balance (1), subject to a battery model (2), (3) and (4), and temperature model (5) and subject to SOC and battery temperature constraints corresponding to the battery operation strategy. Before proceeding, we need to decide on control variables. One obvious control variable is the cooling power  $P_{BTMS}$ . Battery systems can respond quickly to fluctuations in both supply and demand, making them ideal for managing short-term variations and uncertainties in PV generation and load. Conversely, a DG is better suited for providing power over longer periods rather than handling rapid changes. Thus, the variables declared as controls are the DG power  $P_{DG}$  and the excess power  $P_{dump}$ . Battery power adjust accordingly.

Rearranging the power balance, Equation (1), yields

$$\eta_{batt}^{-1} P_{batt}^+ - \eta_{batt} P_{batt}^- = \eta_{PV} \hat{P}_{PV} + P_{DG} - \hat{P}_{load} - P_{BTMS} - P_{dump} =: P_{netto}$$

or, equivalently, using  $P_{netto} = \max\{0, P_{netto}\} - \max\{0, -P_{netto}\}$ ,

$$P_{batt} = P_{batt}^+ - P_{batt}^- = \eta_{batt} \max\{0, P_{netto}\} - \eta_{batt}^{-1} \max\{0, -P_{netto}\} =: P_{brutto} \quad (7)$$

On the other hand, it holds

$$P_{batt} = NP_{cell} = N(V \cdot I) = N(V_{oc} + R_{\tau}I)I = N(V_{oc}I + R_{\tau}I^2). \quad (8)$$

Combining Equation (7) and Equation (8) eventually yields an expression for the current  $I$ ,

$$2R_{\tau}I = -V_{oc} + \sqrt{V_{oc}^2 + 4R_{\tau}N^{-1}P_{brutto}}.$$

The OCP taken into considerations reads as follows. Minimize the DG fuel consumption subject to state equations, and subject to state and final state constraints outlined in the battery operation strategy. The final state constraints (or cycling constraints) are imposed in order to ensure that tomorrow's energy management does not come at the expense of the energy management of the day after tomorrow. More precisely,

$$\min \int_{t_0}^{t_f} P_{DG}(t) dt \quad (9a)$$

$$\text{s.t. } SOC'(t) = \frac{-V_{oc}(SOC) + \sqrt{V_{oc}^2(SOC) + 4R_{\tau}N^{-1}P_{brutto}}}{2R_{\tau}Q_{\tau}} \quad (9b)$$

$$C_{cell}T'_{cell}(t) = R_{\tau}I^2 + U_{cell}(T_{en} - T_{cell}) \quad (9c)$$

$$C_{en}T'_{en}(t) = \eta_{BTMS}P_{BTMS} + N \cdot U_{cell}(T_{cell} - T_{en}) + U_{en}(T_{amb} - T_{en}) \quad (9d)$$

$$SOC(t) \in [SOC^{\min}, SOC^{\max}] \quad \forall t \in [t_0, t_f] \quad (9e)$$

$$T_{cell}(t) \in [T^{\min}, T^{\max}] \quad \forall t \in [t_0, t_f] \quad (9f)$$

$$SOC(t_f) \geq SOC_f \quad (9g)$$

$$T_{cell}(t_f) \leq T_f \quad (9h)$$

We denote  $\mathbf{u} = (\mathbf{u}^{(1)}, \mathbf{u}^{(2)}, \mathbf{u}^{(3)})^T = (P_{BTMS}, P_{DG}, P_{dump})^T$  the control variable and  $\mathbf{x} = (\mathbf{x}^{(1)}, \mathbf{x}^{(2)}, \mathbf{x}^{(3)})^T = (SOC, T_{cell}, T_{en})^T$  the state variable. Accordingly, the OCP reads,

$$\begin{aligned} \min_{\mathbf{u}} \quad & J(\mathbf{u}) = \int_{t_0}^{t_f} \mathbf{u}^{(2)}(t) dt \\ \text{s.t.} \quad & \frac{d\mathbf{x}(t; \mathbf{u})}{dt} = F(t, \mathbf{x}, \mathbf{u}) = A\mathbf{x} + f(t, \mathbf{x}, \mathbf{u}) \\ & \mathbf{x}^{(i)}(t; \mathbf{u}) \in [x_{\min}^{(i)}, x_{\max}^{(i)}] \quad \forall t \in [t_0, t_f], \quad i = 1, 2 \\ & \mathbf{x}^{(1)}(t_f; \mathbf{u}) \geq x_f^{(1)} \\ & \mathbf{x}^{(2)}(t_f; \mathbf{u}) \leq x_f^{(2)} \end{aligned}$$

with

$$A = \begin{pmatrix} 0 & 0 & 0 \\ 0 & -\frac{U_{cell}}{C_{cell}} & \frac{U_{cell}}{C_{cell}} \\ 0 & \frac{N \cdot U_{cell}}{C_{en}} & -\frac{N \cdot U_{cell}}{C_{en}} - \frac{U_{en}}{C_{en}} \end{pmatrix} \quad \text{and} \quad f(t, \mathbf{x}, \mathbf{u}) = \begin{pmatrix} Q_{\tau}^{-1} I(t; \mathbf{x}^{(1)}, \mathbf{u}) \\ \frac{R_{\tau}}{C_{cell}} I^2(t; \mathbf{x}^{(1)}, \mathbf{u}) \\ \frac{\eta_{BTMS} \mathbf{u}^{(1)}}{C_{en}} + \frac{U_{en}}{C_{en}} T_{amb}(t) \end{pmatrix}$$

### Remark 1

1. A battery operation strategy not only asks for SOC and temperature management but also for keeping voltage and current bounded. This is not explicitly included in this work as a consequence of a mini-grid being a low C-rate application resulting in rather low currents and restricting diesel usage. Choosing the interval  $[SOC^{\min}, SOC^{\max}]$  in (4) suitably justifies dropping bounds for the voltage, too.
2. Including a back-up DG asks for the binary decision of switching on and off the generator. This is neglected in this undertaking. The reader is referred to e.g. [?].

## 3.2 Probabilistic problem formulation

Recall the uncertainties PV power  $P_{PV}$ , demand  $P_{load}$  and ambient temperature  $T_{amb}$ . Denote by  $\xi$  the uncertainty. By choice of the control variables, it follows  $P_{netto} = P_{netto}(t; \mathbf{u}, \xi)$  yielding  $I = I(t; \mathbf{x}^{(1)}, \mathbf{u}, \xi)$ . This immediately gives that the uncertainty in the forecasts of solar power and demand translate into uncertainty in the battery SOC dynamics. Similarly, battery temperature becomes uncertain. With a slight abuse of notation, we write

$$\frac{d\mathbf{x}(t; \mathbf{u}, \xi)}{dt} = F(t; \mathbf{x}, \mathbf{u}, \xi)$$

and the state constraints have to take another form for which several possibilities exist. A pretty cheap but not very robust solution is to ask the state to stay bounded in expectation. In contrast, a very robust but also very expensive formulation is to ask the state to stay bounded for every possible realization of the uncertainty. As a good and fair trade-off between robustness and costs, a probabilistic constraint comes into play: we ask the state variable to stay bounded with a given, prescribed probability level (PL). This is the path we will take in this work. To be exact,

$$\min_{\mathbf{u}} J(\mathbf{u}) = \int_{t_0}^{t_f} \mathbf{u}^{(2)}(t) dt$$

subject to the state equations

$$\begin{aligned} \frac{d\mathbf{x}(t; \mathbf{u}, \xi)}{dt} &= F(t; \mathbf{x}, \mathbf{u}, \xi) \\ &= A\mathbf{x} + f(t; \mathbf{x}, \mathbf{u}, \xi) \end{aligned}$$

with

$$A = \begin{pmatrix} 0 & 0 & 0 \\ 0 & -\frac{U_{cell}}{C_{cell}} & \frac{U_{cell}}{C_{cell}} \\ 0 & \frac{N \cdot U_{cell}}{C_{en}} & -\frac{N \cdot U_{cell}}{C_{en}} - \frac{U_{en}}{C_{en}} \end{pmatrix} \quad \text{and} \quad f(t; \mathbf{x}, \mathbf{u}, \xi) = \begin{pmatrix} \frac{1}{Q_r} I(t; \mathbf{x}^{(1)}, \mathbf{u}, \xi) \\ \frac{R_r}{C_{cell}} I^2(t; \mathbf{x}^{(1)}, \mathbf{u}, \xi) \\ \frac{\eta_{BTMS} \mathbf{u}^{(1)}}{C_{en}} + \frac{U_{en}}{C_{en}} T_{amb}(t; \xi) \end{pmatrix}$$

subject to the joint chance constraints (JCCs)

$$\mathbb{P}(\mathbf{x}^{(i)}(t; \mathbf{u}, \xi) \in [x_{\min}^{(i)}, x_{\max}^{(i)}] \quad \forall t \in [t_0, t_f]) \geq p_i, \quad i = 1, 2$$

and subject to the cycling chance constraints (CCCs)

$$\begin{aligned} \mathbb{P}(\mathbf{x}^{(1)}(t_f; \mathbf{u}, \xi) \geq x_f^{(1)}) &\geq q_1 \\ \mathbb{P}(\mathbf{x}^{(2)}(t_f; \mathbf{u}, \xi) \leq x_f^{(2)}) &\geq q_2 \end{aligned}$$

### 3.3 Discretized problem formulation

The approach taken is a first-discretize-then-optimize approach. Therefore, in a first step, a discretization scheme is chosen. Using this discretization, the above ODEs are solved using an implicit Euler scheme. Eventually, the calculation of the gradients of the output equations are discussed. For readability, set

$$\Xi(t; \xi) := (P_{PV}(t; \xi), P_{load}(t; \xi), T_{amb}(t; \xi))^T.$$

Let  $\{t_0, t_1, \dots, t_K = t_f\}$  be an equidistant discretization of the time horizon with  $t_k = t_0 + \frac{t_f - t_0}{K}k$ ,  $k = 1, \dots, K$ . For readability, again, set

$$\begin{aligned} \mathbf{u}_k &= \mathbf{u}(t_k) \\ \Xi_k &= \Xi(t_k; \xi) \\ \mathbf{x}_k &= \mathbf{x}(t_k). \end{aligned}$$

By implicit Euler scheme, the discretized state equations read

$$\begin{aligned} \mathbf{x}_{k+1} &= \mathbf{x}_k + \Delta t \left( A \mathbf{x}_{k+1} + f(t_{k+1}, \mathbf{x}_{k+1}, \mathbf{u}_{k+1}, \Xi_{k+1}) \right), \\ &= \mathbf{x}_k + \Delta t \left( A \mathbf{x}_{k+1} + \hat{f}(t_{k+1} \mathbf{u}_{k+1}, I(\mathbf{x}_{k+1}^{(1)}, \mathbf{u}_{k+1}, \Xi_{k+1}), \Xi_{k+1}) \right), \quad k = 0, \dots, K-1. \end{aligned}$$

Next, we introduce the indices  $\hat{K}^{(i)} = \operatorname{argmax}_k \mathbf{x}_k^{(i)}$  and  $\hat{k}^{(i)} = \operatorname{argmin}_k \mathbf{x}_k^{(i)}$ . It holds for  $i = 1, 2$ ,

$$\begin{aligned} &\mathbf{x}_k^{(i)} \in [x_{\min}^{(i)}, x_{\max}^{(i)}] \quad \forall k = 0, \dots, K \\ \iff &\max_k \mathbf{x}_k^{(i)} - x_{\max}^{(i)} \leq 0 \quad \text{and} \quad x_{\min}^{(i)} - \min_k \mathbf{x}_k^{(i)} \leq 0 \\ \iff &\max \{ \mathbf{x}_{\hat{K}^{(i)}}^{(i)} - x_{\max}^{(i)}, \quad x_{\min}^{(i)} - \mathbf{x}_{\hat{k}^{(i)}}^{(i)} \} \leq 0. \end{aligned}$$

Denote

$$\begin{aligned} g^{(i)}(\mathbf{u}, \xi) &= \max \{ \mathbf{x}_{\hat{K}^{(i)}}^{(i)} - x_{\max}^{(i)}, x_{\min}^{(i)} - \mathbf{x}_{\hat{k}^{(i)}}^{(i)} \}, \quad i = 1, 2 \\ h^{(1)}(\mathbf{u}, \xi) &= x_f^{(1)} - \mathbf{x}_K^{(1)} \\ h^{(2)}(\mathbf{u}, \xi) &= \mathbf{x}_K^{(2)} - x_f^{(2)} \end{aligned}$$

such that the discretized output equations read

$$\begin{aligned} \varphi^{(i)}(\mathbf{u}) &= \mathbb{P}(g^{(i)}(\mathbf{u}, \xi) \leq 0) \geq p_i, \quad i = 1, 2 \\ \gamma^{(i)}(\mathbf{u}) &= \mathbb{P}(h^{(i)}(\mathbf{u}, \xi) \leq 0) \geq q_i, \quad i = 1, 2. \end{aligned}$$

## 4 Spherical-radial decomposition

In order to compute the above probabilities and, within an optimization framework, determine their derivatives, we use the *spherical-radial decomposition* of Gaussian (more generally: elliptically distributed) random vectors. This approach has proven to be very efficient for dealing with chance constraints in comparatively high stochastic dimension and has found numerous applications in operations research and optimal control (e.g., [27, 29, 30, 36]). Its favorable features are strong variance reduction, when compared with methods based on Monte-Carlo sampling ([37, 38]), and the possibility to deal numerically and theoretically with the derivative of the probability function ([22, 28]).

For a centered  $m$ -dimensional Gaussian random vector  $\xi \sim \mathcal{N}(0, \Sigma)$  the spherical-radial decomposition  $\xi = \eta L \zeta$  with  $\eta \sim \chi(m)$  (one-dimensional Chi-distribution with  $m$  degrees of freedom),  $\zeta \sim \mathcal{U}(\mathbb{S}^{m-1})$  (uniform distribution on unit sphere) and  $L$  such that  $LL^T = \Sigma$  holds true. This implies that the Gaussian probability of a measurable set  $M \subseteq \mathbb{R}^m$  may be represented as the spherical integral

$$\int_{v \in \mathbb{S}^{m-1}} \mu_{\eta}(\{r \geq 0 \mid rLv \in M\}) \, d\mu_{\zeta}(v).$$

Applied to a set defined as an inequality  $M = \{z \in \mathbb{R}^m \mid g(u, z) \leq 0\}$  (where  $u$  can be interpreted as a fixed control), this yields that

$$\varphi(u) := \mathbb{P}(g(u, \xi) \leq 0) = \int_{v \in \mathbb{S}^{m-1}} \mu_{\eta}(\{r \geq 0 \mid g(u, rLv) \leq 0\}) \, d\mu_{\zeta}(v).$$

If  $g$  is regular enough, meaning that it is continuous and for each  $v \in \mathbb{S}^{m-1}$  the ray  $\{rLv \mid r \geq 0\}$  enters or leaves the set  $\{z \in \mathbb{R}^m \mid g(u, z) \leq 0\}$  only for a finite number  $n^{u,v}$  of times, this probability can be specified as

$$\varphi(u) = \int_{v \in \mathbb{S}^{m-1}} \sum_{i=1}^{n^{u,v}} \mu_{\eta}([r_i(u, v), R_i(u, v)]) d\mu_{\zeta}(v) \quad (10a)$$

$$= \int_{v \in \mathbb{S}^{m-1}} \sum_{i=1}^{n^{u,v}} [F_{\eta}(R_i(u, v)) - F_{\eta}(r_i(u, v))] d\mu_{\zeta}(v). \quad (10b)$$

Here,  $r_1$  is defined to be the smallest  $r \geq 0$  such that  $g(u, rLv) \leq 0$ . Accordingly, the  $[r_i(u, v), R_i(u, v)]$  are the disjoint intervals describing the intersection of the ray  $\{rLv \mid r \geq 0\}$  with the closed set  $\{z \in \mathbb{R}^m \mid g(u, z) \leq 0\}$ . Note, that the last such interval could be unbounded, hence  $R_{n^{u,v}}(u, v) = \infty$  is possible. In the last formula,  $F_{\eta}$  denotes the cumulative distribution function of the one-dimensional Chi-distribution with  $m$  degrees of freedom. Determining the Gaussian probability of a set in this way rather than by crude Monte Carlo simulation provides estimates with possibly significantly reduced variance, see [37, Section 3.2] and [38, Table 1]. The numerical approximation of the spherical integral involved would result in turning into a finite sum according to an efficient uniform sampling of the unit sphere and by averaging this sum.

If it comes to optimization subject to the chance constraint  $\varphi(u) \geq 0$ , then at least first order information about  $\varphi$  should be available. Differentiability of  $\varphi$  is a delicate issue even in case that all input data of the problem are differentiable. A rigorous verification would rely on a convexity assumption [28] which are not valid in the presence of nonlinear differential equations. We will therefore postulate that it is allowed to interchange differentiation and integration in ():

$$\nabla \varphi(u) = \int_{v \in \mathbb{S}^{m-1}} \sum_{i=1}^{n^{u,v}} [F'_{\eta}(R_i(u, v)) \nabla_u R_i(u, v) - F'_{\eta}(r_i(u, v)) \nabla_u R_i(u, v)] d\mu_{\zeta}(v),$$

where we exploited that the distribution function  $F_{\eta}$  is differentiable with derivative  $F'_{\eta}(t) = f_{\eta}(t)$  and  $f_{\eta}$  being the probability density of the Chi-distribution with  $m$  degrees of freedom. We shall also assume that the endpoint functions  $r_i(u, v), R_i(u, v)$  of the intervals considered above are differentiable with gradients computable via the implicit function theorem. One would then obtain the gradient formulae

$$\nabla_u (r_i/R_i)(u, v) = \frac{\nabla_u g(u, (r_i/R_i)Lv)}{\langle \nabla_z g(u, (r_i/R_i)Lv), Lv \rangle} \quad (i = 1, \dots, n^{u,v}).$$

Altogether, this yields the gradient formula

$$\begin{aligned} \nabla \varphi(u) = \int_{v \in \mathbb{S}^{m-1}} \sum_{i=1}^{n^{u,v}} & \left[ f_{\eta}(R_i(u, v)) \left( \frac{\nabla_u g(u, R_iLv)}{\langle \nabla_z g(u, R_iLv), Lv \rangle} \right) \right. \\ & \left. - f_{\eta}(r_i(u, v)) \left( \frac{\nabla_u g(u, r_iLv)}{\langle \nabla_z g(u, r_iLv), Lv \rangle} \right) \right] d\mu_{\zeta}(v). \end{aligned}$$

As can be seen from the latter equation, for this purpose gradients w.r.t.  $u$  and  $\xi$  have to be computed.

In order to compute the gradient of the individual state variables w.r.t. the control variables, one derives the Jacobian  $\frac{\partial \mathbf{x}_{m^*}}{\partial \mathbf{u}^{(i)}} \in \mathbb{R}^{3 \times K}$ ,  $i \in \{1, 2, 3\}$ . The gradient is computed using the implicit Euler scheme. For readability set

$$\begin{aligned} I_k &= I(t_k, \mathbf{x}_k^{(1)}, \mathbf{u}_k, \Xi_k), \\ \hat{f}_k &= \hat{f}(t_k, \mathbf{u}_k, I_k, \Xi_k). \end{aligned}$$

Using the implicit Euler scheme, one computes for  $k \in \{1, \dots, K\}$  fixed,  $i \in \{1, 2, 3\}$ ,  $l \leq k$ ,

$$\begin{aligned} \frac{\partial \mathbf{x}_k}{\partial \mathbf{u}_l^{(i)}} &= \frac{\partial \mathbf{x}_{k-1}}{\partial \mathbf{u}_l^{(i)}} + \Delta t \left( A \frac{\partial \mathbf{x}_k}{\partial \mathbf{u}_l^{(i)}} + \frac{\partial \hat{f}_k}{\partial \mathbf{u}_l^{(i)}} \right) \\ &= \frac{\partial \mathbf{x}_{k-1}}{\partial \mathbf{u}_l^{(i)}} + \Delta t \left( A \frac{\partial \mathbf{x}_k}{\partial \mathbf{u}_l^{(i)}} + \frac{\partial \hat{f}_k}{\partial \mathbf{u}_k^{(i)}} \frac{\partial \mathbf{u}_k^{(i)}}{\partial \mathbf{u}_l^{(i)}} + \frac{\partial \hat{f}_k}{\partial I_k} \frac{\partial I_k}{\partial \mathbf{u}_l^{(i)}} \right) \\ &= \frac{\partial \mathbf{x}_{k-1}}{\partial \mathbf{u}_l^{(i)}} + \Delta t \left( A \frac{\partial \mathbf{x}_k}{\partial \mathbf{u}_l^{(i)}} + \frac{\partial \hat{f}_k}{\partial \mathbf{u}_k^{(i)}} \frac{\partial \mathbf{u}_k^{(i)}}{\partial \mathbf{u}_l^{(i)}} + \frac{\partial \hat{f}_k}{\partial I_k} \left[ \frac{\partial I_k}{\partial \mathbf{x}_k} \frac{\partial \mathbf{x}_k}{\partial \mathbf{u}_l^{(i)}} + \frac{\partial I_k}{\partial \mathbf{u}_k^{(i)}} \frac{\partial \mathbf{u}_k^{(i)}}{\partial \mathbf{u}_l^{(i)}} \right] \right) \end{aligned}$$

giving

$$\left( I - \Delta t \left[ A + \frac{\partial \hat{f}_k}{\partial I_k} \frac{\partial I_k}{\partial \mathbf{x}_k} \right] \right) \frac{\partial \mathbf{x}_k}{\partial \mathbf{u}_l^{(i)}} = \frac{\partial \mathbf{x}_{k-1}}{\partial \mathbf{u}_l^{(i)}} + \Delta t \left[ \frac{\partial \hat{f}_k}{\partial \mathbf{u}_k^{(i)}} + \frac{\partial \hat{f}_k}{\partial I_k} \frac{\partial I_k}{\partial \mathbf{u}_k^{(i)}} \right] \delta_{k,l}$$

eventually yielding Algorithm 1.



---

```

for  $l = 1, \dots, K$  do
    if  $l \leq m^*$  then
        Compute  $\frac{\partial \mathbf{x}_l}{\partial \mathbf{u}_l^{(i)}}$  by solving
    
```

$$\left( I - \Delta t \left[ A + \frac{\partial \hat{f}_l}{\partial I_l} \frac{\partial I_l}{\partial \mathbf{x}_l} \right] \right) \frac{\partial \mathbf{x}_l}{\partial \mathbf{u}_l^{(i)}} = \Delta t \left[ \frac{\partial \hat{f}_l}{\partial \mathbf{u}_l^{(i)}} + \frac{\partial \hat{f}_l}{\partial I_l} \frac{\partial I_l}{\partial \mathbf{u}_l^{(i)}} \right]$$

```

        for  $k = l + 1, \dots, m^*$  do
            Compute  $\frac{\partial \mathbf{x}_k}{\partial \mathbf{u}_l^{(i)}}$  by solving
    
```

$$\left( I - \Delta t \left[ A + \frac{\partial \hat{f}_k}{\partial I_k} \frac{\partial I_k}{\partial \mathbf{x}_k} \right] \right) \frac{\partial \mathbf{x}_k}{\partial \mathbf{u}_l^{(i)}} = \frac{\partial \mathbf{x}_{k-1}}{\partial \mathbf{u}_l^{(i)}}$$

```

        end for
    else
        Set  $\frac{\partial \mathbf{x}_{m^*}}{\partial \mathbf{u}_l^{(i)}} = 0$ .
    end if
end for

```

---

### Algorithm 1 Computation of $\frac{\partial \mathbf{x}_{m^*}}{\partial \mathbf{u}^{(i)}}$

As before, to compute the gradient w.r.t. the uncertainties, one derives the Jacobian  $\frac{\partial \mathbf{x}_{m^*}}{\partial \xi} \in \mathbb{R}^{3 \times m}$  and then restricts to the respective row yielding. Again, one computes the gradient w.r.t.  $\xi$  using the implicit Euler scheme. For  $k \in \{1, \dots, K\}$  fixed

$$\begin{aligned} \frac{\partial \mathbf{x}_k}{\partial \xi} &= \frac{\partial \mathbf{x}_{k-1}}{\partial \xi} + \Delta t \left( A \frac{\partial \mathbf{x}_k}{\partial \xi} + \frac{\partial \hat{f}_k}{\partial \xi} \right) \\ &= \frac{\partial \mathbf{x}_{k-1}}{\partial \xi} + \Delta t \left( A \frac{\partial \mathbf{x}_k}{\partial \xi} + \frac{\partial \hat{f}_k}{\partial \Xi_k} \frac{\partial \Xi_k}{\partial \xi} + \frac{\partial \hat{f}_k}{\partial I_k} \frac{\partial I_k}{\partial \xi} \right) \\ &= \frac{\partial \mathbf{x}_{k-1}}{\partial \xi} + \Delta t \left( A \frac{\partial \mathbf{x}_k}{\partial \xi} + \frac{\partial \hat{f}_k}{\partial \Xi_k} \frac{\partial \Xi_k}{\partial \xi} + \frac{\partial \hat{f}_k}{\partial I_k} \left[ \frac{\partial I_k}{\partial \mathbf{x}_k} \frac{\partial \mathbf{x}_k}{\partial \xi} + \frac{\partial I_k}{\partial \Xi_k} \frac{\partial \Xi_k}{\partial \xi} \right] \right) \end{aligned}$$

giving

$$\left( I - \left[ \Delta t A + \frac{\partial \hat{f}_k}{\partial I_k} \frac{\partial I_k}{\partial \mathbf{x}_k} \right] \right) \frac{\partial \mathbf{x}_k}{\partial \xi} = \frac{\partial \mathbf{x}_{k-1}}{\partial \xi} + \Delta t \left( \frac{\partial \hat{f}_k}{\partial \Xi_k} \frac{\partial \Xi_k}{\partial \xi} + \frac{\partial \hat{f}_k}{\partial I_k} \frac{\partial I_k}{\partial \Xi_k} \frac{\partial \Xi_k}{\partial \xi} \right)$$

eventually yielding Algorithm 2.

Set  $\frac{\partial \mathbf{x}_0}{\partial \xi} = 0 \in \mathbb{R}^{3 \times m}$ .

**for**  $k = 1, \dots, m^*$  **do**

    Compute  $\frac{\partial \mathbf{x}_k}{\partial \xi}$  by solving

$$\left( I - \left[ \Delta t A + \frac{\partial \hat{f}_k}{\partial I_k} \frac{\partial I_k}{\partial \mathbf{x}_k} \right] \right) \frac{\partial \mathbf{x}_k}{\partial \xi} = \frac{\partial \mathbf{x}_{k-1}}{\partial \xi} + \Delta t \left( \frac{\partial \hat{f}_k}{\partial \Xi_k} \frac{\partial \Xi_k}{\partial \xi} + \frac{\partial \hat{f}_k}{\partial I_k} \frac{\partial I_k}{\partial \Xi_k} \frac{\partial \Xi_k}{\partial \xi} \right)$$

**end for**

**Algorithm 2** Computation of  $\frac{\partial \mathbf{x}_{m^*}}{\partial \xi}$

**Remark 2** Although we are not able to formally derive the differentiability of  $\varphi$ , numerical practice shows that differentiability is likely to hold. In particular, one could alternatively run an optimization solver without exploiting gradient information, just based on function values of the probability function. Then, one would arrive at the same solutions but at the expense of much higher computing times.

## 5 Numerical results

In this section, we present the numerical results obtained by solving the optimal control problem. For this purpose, the optimal control problem is understood as a constrained optimization problem after discretization, which is then solved using the Python library SciPy [39]. The time required for one iteration of the optimization routine depends significantly on the sample size. For  $2^{16}$  samples, one iteration step takes approximately 2 to 3 minutes.

In a very first step, the mini-grid design has to be determined. Special attention should be paid to the integration of BESS, its sizing and its operation strategy. In a second step, the uncertainties are introduced. Eventually, the results will be presented and discussed critically with a focus on the lack of systematic methodology for sizing as a long-term planning issue and corresponding room for improvement in order to ensure optimal performance.

### 5.1 Assumptions

Given a demand profile, PV output power can be scaled such that, integrated over time, they are roughly equal. After having decided on a battery operation strategy and having at hand demand and PV power profiles, the BESS can be sized, i.e. the number of cells  $N$  the BESS consists of can be determined.

For the sake of sizing, we thus have to agree on a battery operation strategy, i.e. we have to agree on bounds  $[SOC^{\min}, SOC^{\max}]$  for the SOC. We recall that battery degradation is accelerated the higher the DOD is. For the SOC we choose to follow the standard

$$[SOC^{\min}, SOC^{\max}] = [0.2, 0.8]. \quad (11)$$

The number of battery cells found to work well and used in this work is  $N = 17\,500$ . We recall that higher temperatures also favor battery degradation. Hence, for battery thermal operation strategy, we choose not to follow the widely accepted recommendation [40] of  $[T^{\min}, T^{\max}] = [15^\circ\text{C}, 35^\circ\text{C}]$ . For mini-grid operation, choosing a narrower temperature range aligns well with optimizing performance and ensuring longevity since managing battery temperature within the desired range is achievable without excessive energy consumption. This is due to a mini-grid being a low C-rate application resulting in little Joule heat being generated compared to a high C-rate application. Hence, we choose

$$[T^{\min}, T^{\max}] = [20^\circ\text{C}, 25^\circ\text{C}]. \quad (12)$$

Finally, we impose  $SOC_f = 0.5$  and  $T_f = 22.5^\circ\text{C}$ . Throughout this section, the same uncertain demand  $P_{load}$  and the same uncertain ambient temperature  $T_{amb}$  is assumed; compare to Figure 4a and Figure 4b, respectively. For PV power, two scenarios are taken into consideration: a very sunny day, as shown in Figure 4c and a partly cloudy day, as illustrated in Figure 4d.

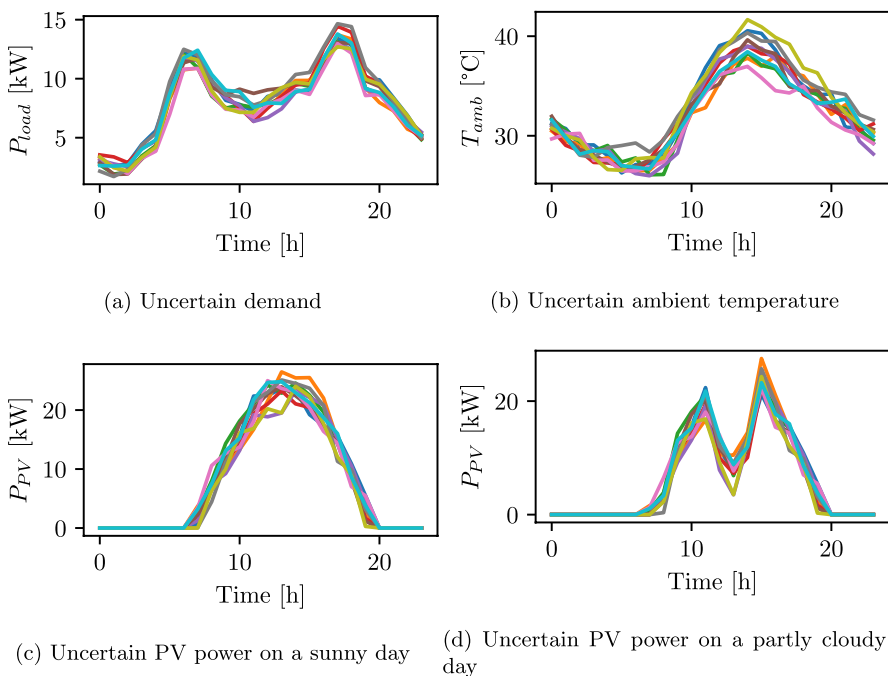
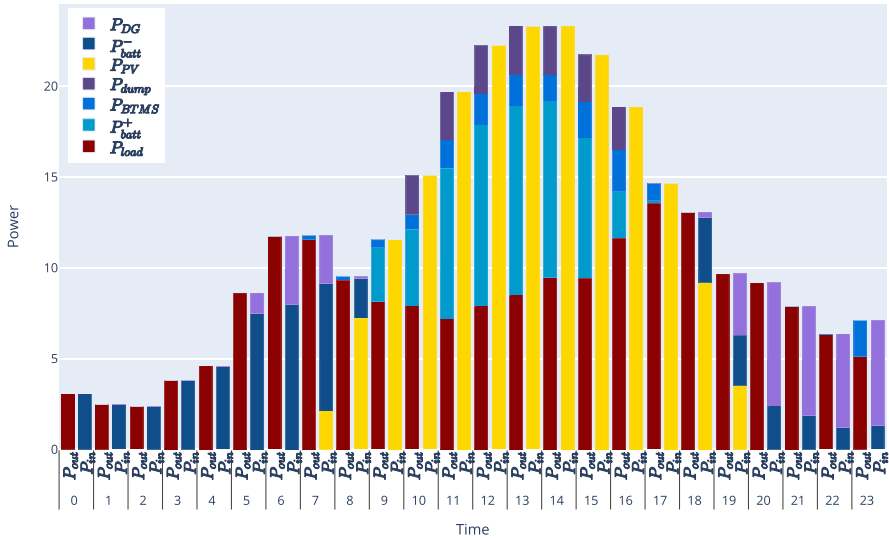
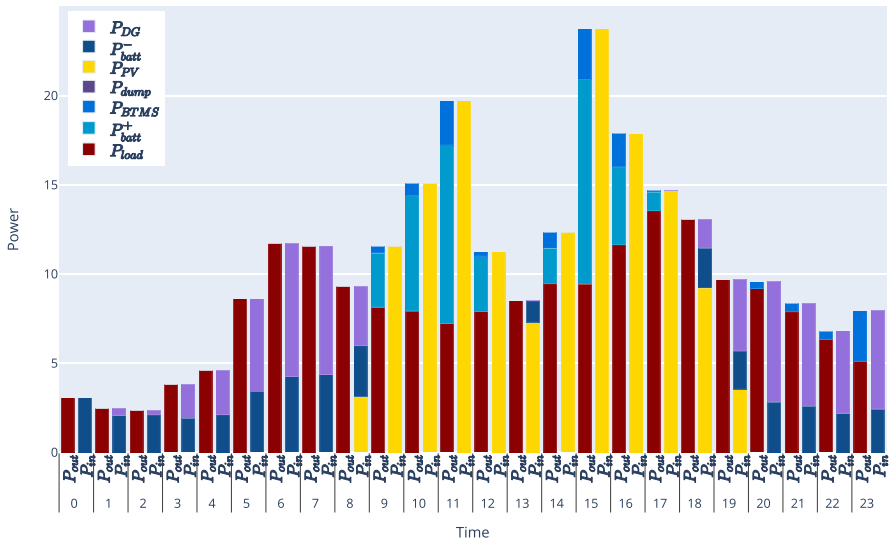


**Fig. 4** Realization of the uncertainties



(a) On a sunny day



(b) On a partly cloudy day

**Fig. 5** Power balance for  $p_1 = p_2 = 0.95$ ,  $q_1 = q_2 = 0.75$  for the forecasts  $\hat{P}_{PV}$ ,  $\hat{P}_{load}$  and  $\hat{T}_{amb}$

## 5.2 Results and discussion

The proposed energy management strategies illustrated in Figure 5 are each result of solving the discretized probabilistic OCP numerically w.r.t. increasing joint PLs  $p = p_i \in \{0.5, 0.75, 0.95\}$  and cycling PLs  $q = q_i = \min\{0.75, p_i\}$ ,  $i = 1, 2$ . The

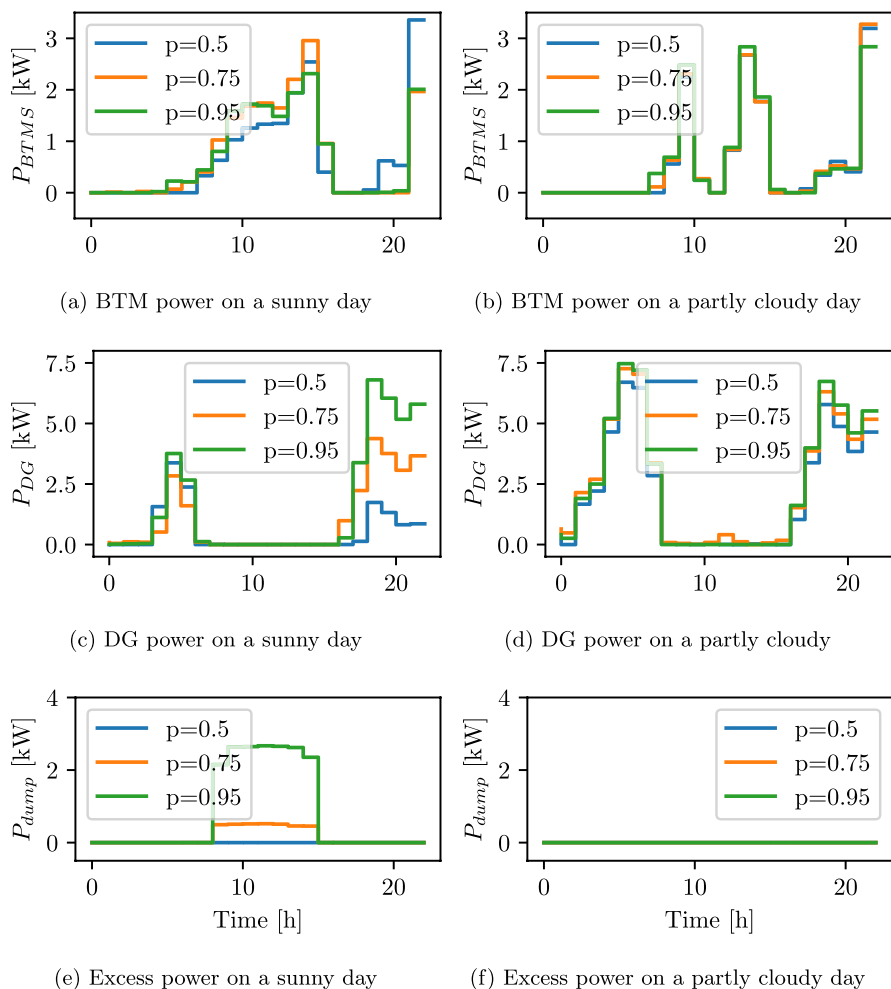


**Fig. 6** Optimized control variables for different joint probability levels  $p$ . The cycling probability levels are given by  $q = \min \{0.75, p\}$

**Table 3** Prescribed and realized probability levels for SOC and battery cell temperature on a sunny day. Printed in bold: binding probability level.

$\mathbb{P}(SOC(t) \in [0.2, 0.8] \forall t)$	$p_1$	$\mathbb{P}(SOC(t_f) \geq 0.5)$	$q_1$
<b>0.5</b>	<b>0.5</b>	<b>0.5</b>	<b>0.5</b>
<b>0.75</b>	<b>0.75</b>	<b>0.75</b>	<b>0.75</b>
<b>0.95</b>	<b>0.95</b>	<b>0.75</b>	<b>0.75</b>
$\mathbb{P}(T_{cell}(t) \in [20, 25] \forall t)$	$p_2$	$\mathbb{P}(T_{cell}(t_f) \leq 22.5)$	$q_2$
<b>0.5</b>	<b>0.5</b>	<b>0.5</b>	<b>0.5</b>
<b>0.75</b>	<b>0.75</b>	<b>0.75</b>	<b>0.75</b>
<b>0.95</b>	<b>0.95</b>	<b>0.75</b>	<b>0.75</b>

reader is referred to Table 1 and Table 2 for the thermodynamic parameters used for the numerical simulations.

The optimized control variables considering a sunny day are illustrated in Figures 6a, 6c, and 6e and the resulting state variables are depicted in Figure 8. Prescribed and actual (realized) PLs can be found in Table 3. Similarly, the optimized control variables for a partly cloudy day are depicted in Figures 6b, 6d and 6f, and the resulting state variables are depicted in Figure 9. Prescribed and actual (realized) PLs can be found in Table 4. A depiction of the power balance for sunny and partly cloudy day for the forecast can be seen in Figure 5a and Figure 5b, respectively.

On a sunny day, generally, the higher the desired reliability, the higher the usage of the DG and the higher the amount of excess power that has to be dumped as becomes very evident from Figure 6c and Figure 6e. In the early morning, when there is no PV power available, the DG has to be switched on in order to not violate the JCC on SOC by falling (in too many scenarios) below the lower bound on SOC. During mid-day, when there is PV power available, increasing the joint PL  $p_1$  means that the amount of excess power  $P_{dump}$  to be dumped increases in order to not over-charge the battery (too frequently). The DG is switched on again in the evening due to the imposed CCC on SOC. The usage of DG in the evening increases even for non-increasing cycling PL  $q_1$  as the joint PL  $p_1$  is nonetheless rising: the excess power that has to be dumped in the (after-)noon is then missing in the evening again. Cooling takes place mostly during mid-day when there is PV power available and when it is hottest. At a first glance, there seems to be no clear ordering w.r.t. reliability level, cf. Figure 6e. Taking a very close look reveals that the overall cooling power increases until the joint PL  $p_2$  on battery temperature reaches a value of 0.75 and then starts to decrease. This is due to the cycling PL  $q_2$  being kept constant after having reached a value of  $q_2 = 0.75$ . Simultaneously, the higher the joint PL  $p_2$ , the higher the cooling power in the early morning in order to not exceed the upper bound (too often). In the afternoon, cooling power is lower for higher joint PL  $p_2$  in a maximal possible way without violating the JCC on the lower bound. For cooling in the evening, the DG has to run again. Thus, cooling is performed in the afternoon as much as possible such that the JCC on battery temperature is still met, i.e. the lower bound on battery temperature is not violated (too frequently).

Also on a partly cloudy day, generally, the higher the desired reliability, the higher the usage of DG, see Figure 6d. In contrast, there is no excess power at all for any PL, compare to Figure 6f. An important observation is that PLs on the JCC of SOC are not binding until very high probabilities. This is due to the CCC on SOC being the driving force: the higher the PL  $q_1$  on the CCC, the more DG power has to be

**Table 4** Prescribed and realized probability levels for SOC and battery cell temperature on a partly cloudy day. Printed in bold: binding probability levels

$\mathbb{P}(SOC(t) \in [0.2, 0.8] \forall t)$	$p_1$	$\mathbb{P}(SOC(t_f) \geq 0.5)$	$q_1$
0.97	0.5	<b>0.5</b>	<b>0.5</b>
0.93	0.75	<b>0.75</b>	<b>0.75</b>
<b>0.95</b>	<b>0.95</b>	<b>0.75</b>	<b>0.75</b>
$\mathbb{P}(T_{cell}(t) \in [20, 25] \forall t)$	$p_2$	$\mathbb{P}(T_{cell}(t_f) \leq 22.5)$	$q_2$
<b>0.5</b>	<b>0.5</b>	<b>0.5</b>	<b>0.5</b>
<b>0.75</b>	<b>0.75</b>	<b>0.75</b>	<b>0.75</b>
<b>0.95</b>	<b>0.95</b>	<b>0.75</b>	<b>0.75</b>

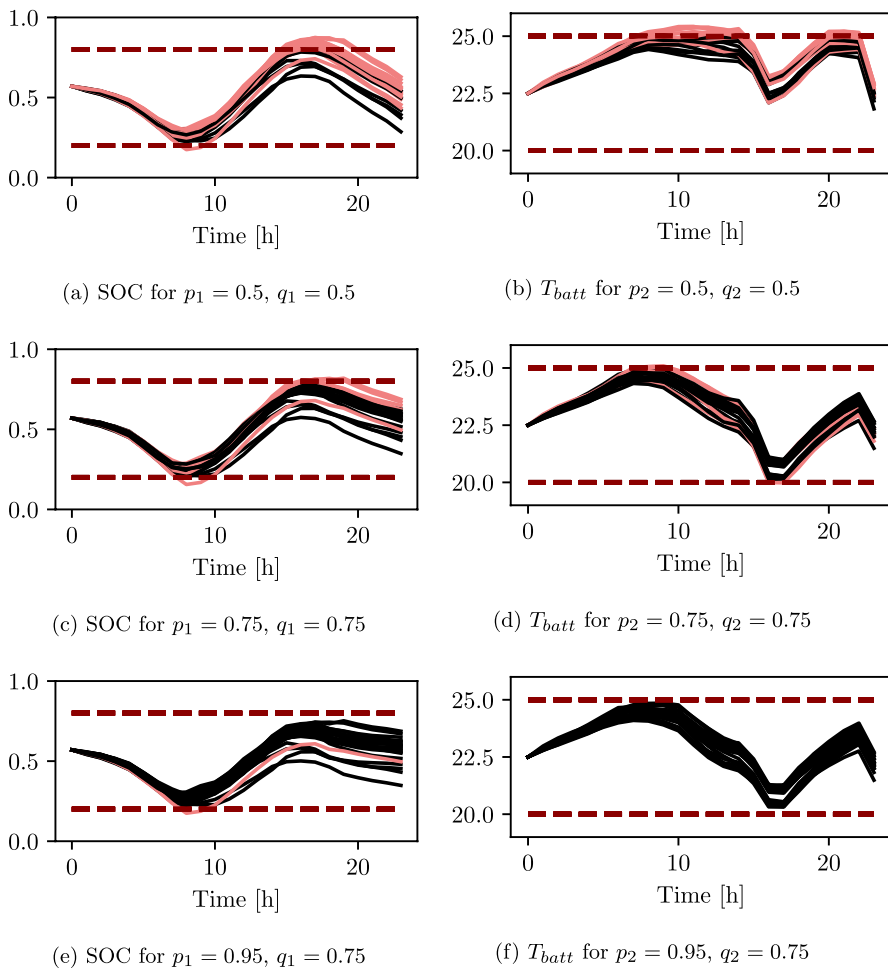


**Fig. 8** State variables on a sunny day. A total of 20 trajectories is plotted each. Black: trajectories that satisfy the joint chance constraint. Red: trajectories that do not satisfy the joint chance constraint

imported. Thus, the higher the cycling PL, the lower the realized probability for the JCC as the upper bound becomes active. This can be seen from Table 4. The CCC being the driving force is highlighted in Figure 7b, where the objective increases until  $PL\ q_i = p_i = 0.75, i = 1, 2$  and afterwards nearly stays constant – as the cycling PL stays constant, too. Cooling is performed in a way that is just enough: the upper bound on battery temperature is the active one and cooling increases with increasing joint PL.

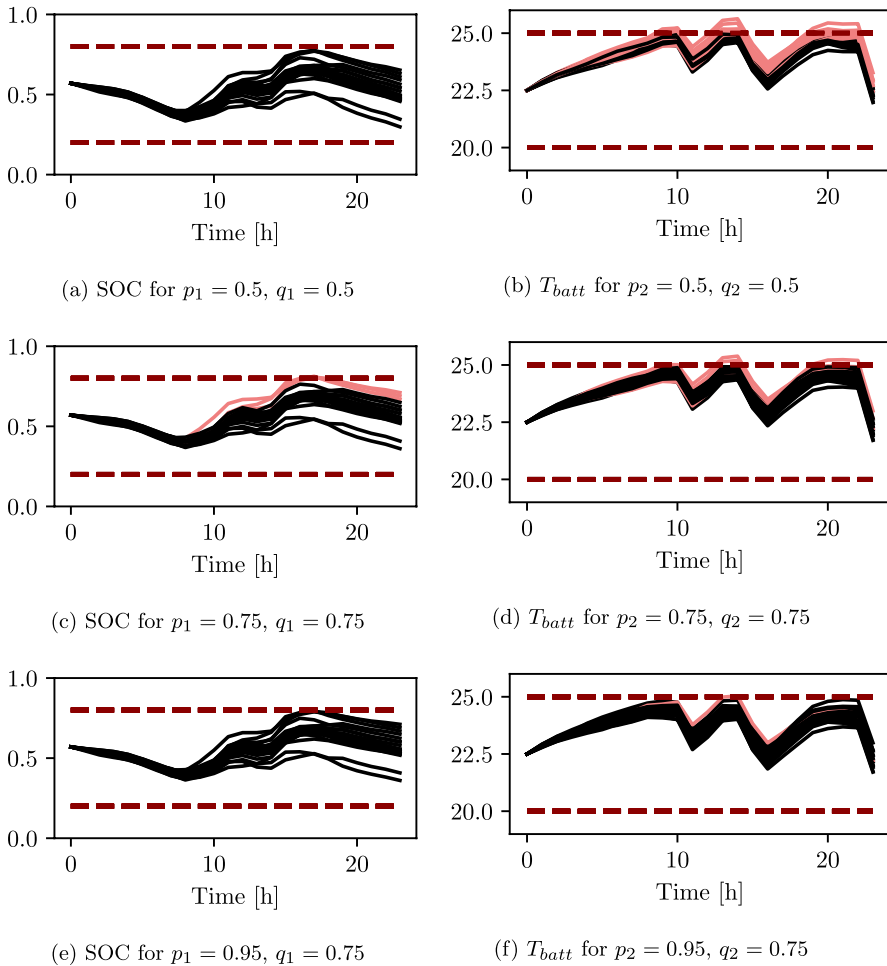


**Fig. 9** State variables on a partly cloudy day. A total of 20 trajectories is plotted each. Black: trajectories that satisfy the joint chance constraint. Red: trajectories that do not satisfy the joint chance constraint

### 5.3 Conclusion and outlook

Given the task of finding an optimal energy management strategy for an isolated mini-grid, a probabilistic OCP taking into account has been set up and solved numerically using the concept of chance constraints.

As evident from Figure 7, the partly cloudy day comes at higher cost due to augmented need for DG power. DG usage on a partly cloudy day is driven by meeting the CCC on SOC. On a sunny day, compared to a partly cloudy day, there is an excess of power that needs to be dumped. Cooling on a sunny day is conducted such that cooling is minimal in the evening as for cooling in the evening the DG has to run. On a partly cloudy day cooling power is just enough to meet the JCC and CCC on battery temperature. The reader's attention is drawn to the following. Fuel consumption



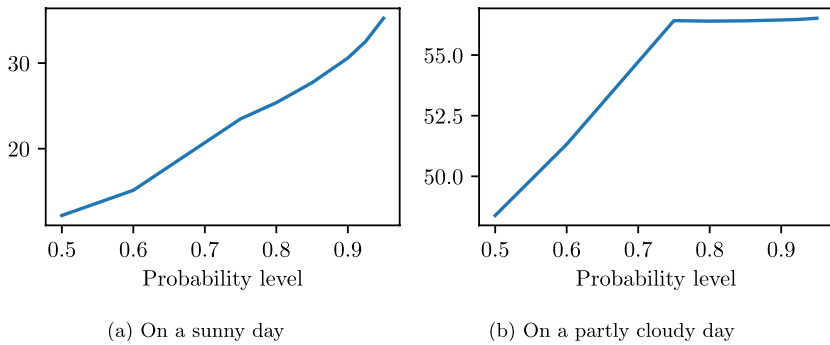


**Fig. 7** Total DG power needed as a function of joint PL  $p = p_1 = p_2$ . The cycling PL  $q = q_1 = q_2$  is given by  $q = \min \{p, 0.75\}$

of the DG could be further refined. In addition, by introducing binary variables for switching on and off the DG, ramp-up rates of the DG can be included: a cold DG does not run as efficiently as a warm one [8].

To classify these results, we can compare them to the deterministic optimization problem that takes into account the expected values of the forecasts. For instance, on a sunny day, the total DG power for that optimization, is around 20.95 kW and yields the subsequent probabilities. The bounds on SOC are maintained with a probability of  $\mathbb{P}(SOC(t) \in [0.2, 0.8] \forall t) = 0.48$ , and the bounds on battery temperature are maintained with a probability of  $\mathbb{P}(T_{cell}(t) \in [20, 25] \forall t) = 0.33$ . In contrast, with a moderate change in the objective, we can achieve a very high level of reliability. For example, asking  $p_1 = p_2 = 0.9$  comes at a total DG power usage of 30.59 kW.

The numerical results presented in the previous section indicate that the probabilistic OCP delivers an energy management strategy that strikes balance between reliability and cost. The higher the PL, the higher the operational costs and the operator may decide, based on these findings, which strategy and which reliability level to choose. The results indicate that the solution concept presented in this paper offers a generic good way of optimizing energy management. Nonetheless, the resulting energy management strategy heavily depends on the choice of parameters.

There are a bunch of open questions. As usage of the DG is pretty high and as there is even an excess of power at some times, this indicates that the BESS is not sized very well. Also, deciding on battery (thermal) operation strategies can potentially be improved. This indicates that sizing and designing mini-grids and their operation can be further enhanced. This is ongoing work: set up and study a two-time scale optimization problem including battery degradation dynamics for the optimal design, i.e. layout and operation strategies, of stand-alone mini-grids.

**Funding** This work was funded by the German Research Foundation (DFG) under the German National Excellence Strategy - The Berlin Mathematics Research Center MATH+ (EXC-2046) in Project AA4-10.

**Data availability** Data will be made available on reasonable request.

## Declarations

**Conflict of interest** The authors have no conflicts of interest to declare that are relevant to the content of this article.

## References

- Hannan, M.A., Al-Shetwi, A., Begum, R.A., Young, S.E., Hoque, M.M., Ker, P., Mansur, M., Alzaareer, K.: The value of thermal management control strategies for battery energy storage in grid decarbonization: Issues and recommendations. *J. Clean. Prod.* 276, 124223 (2020) <https://doi.org/10.1016/j.jclepro.2020.124223>
- Rahimi-Eichi, H., Ojha, U., Baronti, F., Chow, M.: Battery management system: An overview of its application in the smart grid and electric vehicles. *IEEE Ind. Electron. Mag.* 7(2), 4–16 (2013). <https://doi.org/10.1109/MIE.2013.2250351>
- Ecker, M., Nieto, N., Käbitz, S., Schmalstieg, J., Blanke, H., Warnecke, A., Sauer, D.W.: Calendar and cycle life study of  $\text{Li}(\text{NiMnCo})\text{O}_2$ -based 18650 lithium-ion batteries. *J. Power Sources* 248, 839–851 (2014). <https://doi.org/10.1016/j.jpowsour.2013.09.143>
- Schmalstieg, J., Käbitz, S., Ecker, M., Sauer, D.U.: A holistic aging model for  $\text{Li}(\text{NiMnCo})\text{O}_2$  based 18650 lithium-ion batteries. *J. Power Sources* 257, 325–334 (2014). <https://doi.org/10.1016/j.jpowsour.2014.02.012>
- Lander, L., Kallitsis, E., Hales, A., Edge, J.S., Korre, A., Offer, G.: Cost and carbon footprint reduction of electric vehicle lithium-ion batteries through efficient thermal management. *Appl. Energy* 289, 116737 (2021). <https://doi.org/10.1016/j.apenergy.2021.116737>
- Plett, G.: *Battery Management Systems, Volume I: Battery Modeling*. Power engineering/power electronics. Artech House, Norwood, MA (2015)
- Rosewater, D.M., Copp, D.A., Nguyen, T.A., Byrne, R.H., Santoso, S.: Battery energy storage models for optimal control. *IEEE Access* 7, 178357–178391 (2019). <https://doi.org/10.1109/ACCESS.2019.2957698>
- Palma-Behnke, R., Benavides, C., Lanas, F., Severino, B., Reyes, L., Llanos, J., Saez, D.: A microgrid energy management system based on the rolling horizon strategy. *IEEE Trans. Smart Grid* 4(2), 996–1006 (2013). <https://doi.org/10.1109/tsg.2012.2231440>
- Luu, N.A., Tran, Q.-T., Bacha, S.: Optimal energy management for an island microgrid by using dynamic programming method. In: 2015 IEEE Eindhoven PowerTech, pp. 1–6. IEEE, ??? (2015). <https://doi.org/10.1109/ptc.2015.7232678>
- Taha, M.S., Abdeltawab, H.H., Mohamed, Y.A.-R.I.: An online energy management system for a grid-connected hybrid energy source. *IEEE J. Emerg. Sel. Topics Power Electron.* 6(4), 2015–2030 (2018) <https://doi.org/10.1109/jestpe.2018.2828803>
- Rosewater, D., Baldick, R., Santoso, S.: Risk-averse model predictive control design for battery energy storage systems. *IEEE Trans. Smart Grid* 11(3), 2014–2022 (2020). <https://doi.org/10.1109/tsg.2019.2946130>
- Charnes, A., Cooper, W.W.: Chance-constrained programming. *Manag. Sci.* 6(1), 73–79 (1959). <https://doi.org/10.1287/mnsc.6.1.73>. Accessed 2024-04-29
- Prékopa, A.: *Stochastic Programming. Mathematics and its applications*; v. 324. Kluwer Academic Publishers, Dordrecht (1995). <https://doi.org/10.1007/978-94-017-3087-7>
- Campi, M.C., Garatti, S.: The exact feasibility of randomized solutions of uncertain convex programs. *SIAM J. Optim.* 19(3), 1211–1230 (2008)
- Pagnoncelli, B.K., Ahmed, S., Shapiro, A.: Sample average approximation method for chance constrained programming: Theory and applications. *J. Optim. Theory Appl.* 142, 399–416 (2009)
- Nemirovski, A., Shapiro, A.: Convex approximations of chance constrained programs. *SIAM J. Optim.* 17(4), 969–996 (2006)
- Hong, L.J., Yang, Y., Zhang, L.: Sequential convex approximations to joint chance constrained programs: A monte carlo approach. *Oper. Res.* 59, 617–630 (2011)
- Peña-Ordieres, A., Luedtke, J.R., Wächter, A.: Solving chance-constrained problems via a smooth sample-based nonlinear approximation. *SIAM J. Optim.* 30, 2221–2250 (2020)

19. Geletu, A., Hoffmann, A., Klöppel, M., Li, P.: An inner-outer approximation approach to chance constrained optimization. *SIAM J. Optim.* **27**, 1834–1857 (2017)
20. Caillaud, J.-B., Cerf, M., Sassi, A., Trélat, E., Zidani, H.: Solving chance constrained optimal control problems in aerospace via kernel density estimation. *Optim. Control Appl. Methods* **39**(5), 1833–1858 (2018)
21. Schuster, M., Strauch, E., Gugat, M., Lang, J.: Probabilistic constrained optimization on flow networks. *Optim. Eng.* **23**(2), 1–50 (2022)
22. Ackooij, W., Henrion, R.: Gradient formulae for nonlinear probabilistic constraints with Gaussian and Gaussian-like distributions. *SIAM J. Optim.* **24**(4), 1864–1889 (2014). <https://doi.org/10.1137/130922689>
23. Barrera, J., Homem-de-Mello, T., Moreno, E., Pagnoncelli, B.K., Canessa, G.: Chance-constrained problems and rare events: an importance sampling approach. *Math. Program.* **157**, 153–189 (2016)
24. Tong, S., Subramanyam, A., Rao, V.: Optimization under rare chance constraints. *SIAM J. Optim.* **32**, 930–958 (2022)
25. Liu, G., Starke, M., Xiao, B., Zhang, X., Tomsovic, K.: Microgrid optimal scheduling with chance-constrained islanding capability. *Electric Power Syst. Res.* **145**, 197–206 (2017) <https://doi.org/10.1016/j.epsr.2017.01.014>
26. Zhao, B., Shi, Y., Dong, X., Luan, W., Bornemann, J.: Short-term operation scheduling in renewable-powered microgrids: A duality-based approach. *IEEE Trans. Sustain. Energy* **5**(1), 209–217 (2014). <https://doi.org/10.1109/TSTE.2013.2279837>
27. Ouanes, N., González Grandín, T., Heitsch, H., Henrion, R.: Optimizing the Economic Dispatch of Weakly-connected Mini-grids Under Uncertainty Using Joint Chance Constraints. Preprint no. 3069 (2023), Weierstrass Institute Berlin
28. Ackooij, W., Henrion, R.: (sub-)gradient formulae for probability functions of random inequality systems under Gaussian distribution. *J. Uncertain. Quantif.* **5**, 63–87 (2017) <https://doi.org/10.1137/16M1061308>
29. Heitsch, H.: On probabilistic capacity maximization in a stationary gas network. *Optimization* **69**(3), 575–604 (2019) <https://doi.org/10.1080/02331934.2019.1625353>
30. Pérez-Aros, P., Quiñao, C., Tejo, M.: Control in probability for sde models of growth population. *Appl. Math. Optim.* **86**(44) (2022) <https://doi.org/10.1007/s00245-022-09915-7>
31. Halliday, D., Resnick, R., Walker, J.: *Fundamentals of Physics*. John Wiley & Sons Canada, Limited, New York (2010)
32. Engels, J., Claessens, B., Deconinck, G.: Techno-economic analysis and optimal control of battery storage for frequency control services, applied to the german market. *Appl. Energy* **242**, 1036–1049 (2019) <https://doi.org/10.1016/j.apenergy.2019.03.128>
33. Drake, S.J., Wetz, D.A., Ostanek, J.K., Miller, S.P., Heinzl, J.M., Jain, A.: Measurement of anisotropic thermophysical properties of cylindrical li-ion cells. *J. Power Sources* **252**, 298–304 (2014). <https://doi.org/10.1016/j.jpowsour.2013.11.107>
34. Shumway, R.H., Stoffer, D.S.: *Time Series Analysis and Its Applications*. Springer Texts in Statistics. Springer, Cham (2000). <https://doi.org/10.1007/978-3-319-52452-8>
35. Rad, M.A.V., Kasacian, A., Niu, X., Zhang, K., Mahian, O.: Excess electricity problem in off-grid hybrid renewable energy systems: A comprehensive review from challenges to prevalent solutions. *Renew. Energy* **212**, 538–560 (2023). <https://doi.org/10.1016/j.renene.2023.05.073>
36. Farshbaf-Shaker, M.H., Gugat, M., Heitsch, H., Henrion, R.: Optimal neumann boundary control of a vibrating string with uncertain initial data and probabilistic terminal constraints. *SIAM J. Control. Optim.* **58**(4), 2288–2311 (2020). <https://doi.org/10.1137/19m1269944>
37. Henrion, R., Stadler, G., Wechsung, F.: Optimal control under uncertainty with joint chance state constraints: almost-everywhere bounds, variance reduction, and application to (bi-)linear elliptic PDEs. *arXiv* (2024). <https://doi.org/10.48550/ARXIV.2412.05125>
38. Gotzes, C., Heitsch, H., Henrion, R., Schultz, R.: On the quantification of nomination feasibility in stationary gas networks with random load. *Math. Methods Oper. Res.* **84**, 427–457 (2016) <https://doi.org/10.1007/s00186-016-0564-y>

39. Virtanen, P., Gommers, R., Oliphant, T.E., Haberland, M., Reddy, T., Cournapeau, D., Burovski, E., Peterson, P., Weckesser, W., Bright, J., van der Walt, S.J., Brett, M., Wilson, J., Millman, K.J., Mayorov, N., Nelson, A.R.J., Jones, E., Kern, R., Larson, E., Carey, C.J., Polat, İ., Feng, Y., Moore, E.W., VanderPlas, J., Laxalde, D., Perktold, J., Cimrman, R., Henriksen, I., Quintero, E.A., Harris, C.R., Archibald, A.M., Ribeiro, A.H., Pedregosa, F., van Mulbregt, P., SciPy 1.0 Contributors: SciPy 1.0: Fundamental Algorithms for Scientific Computing in Python. *Nat. Methods* 17, 261–272 (2020) <https://doi.org/10.1038/s41592-019-0686-2>
40. Ma, S., Jiang, M., Tao, P., Song, C., Wu, J., Wang, J., Deng, T., Shang, W.: Temperature effect and thermal impact in lithium-ion batteries: A review. *Prog. Nat. Sci.: Mater. Int.* 28(6), 653–666 (2018) <https://doi.org/10.1016/j.pnsc.2018.11.002>

**Publisher's Note** Springer Nature remains neutral with regard to jurisdictional claims in published maps and institutional affiliations.

Springer Nature or its licensor (e.g. a society or other partner) holds exclusive rights to this article under a publishing agreement with the author(s) or other rightsholder(s); author self-archiving of the accepted manuscript version of this article is solely governed by the terms of such publishing agreement and applicable law.

## Authors and Affiliations

Nina Kliche<sup>1</sup>  · René Henrion<sup>1</sup> · Dietmar Hömberg<sup>1,2,3</sup>

✉ Nina Kliche  
nina.kliche@wias-berlin.de

René Henrion  
rene.henrion@wias-berlin.de

Dietmar Hömberg  
dietmar.hoemberg@wias-berlin.de

<sup>1</sup> Weierstrass Institute for Applied Analysis and Stochastics, Mohrenstr. 39, 10117 Berlin, Germany

<sup>2</sup> Institute of Mathematics, Technical University Berlin, Str. des 17. Juni 136, 10623 Berlin, Germany

<sup>3</sup> Department of Mathematical Sciences, Norwegian University of Science and Technology, Alfred Getz' vei 1, 7034 Trondheim, Norway